INTERNATIONAL JOURNAL FOR NUMERICAL METHODS IN ENGINEERING
Int. J. Numer. Meth. Engng 2002; **53**:1353–1376 (DOI: 10.1002/nme.340)

Higher-order responses of three-dimensional elastic plate structures and their numerical illustration by *p*-FEM

Monique Dauge[1], Andreas Rössle[2] and Zohar Yosibash[3,*,†]

[1] *Institut Mathématique, UMR 6625 du CNRS, Université de Rennes 1, Campus de Beaulieu, 35042 Rennes, France*
[2] *Mathematisches Institut A, Universität Stuttgart, Pfaffenwaldring 57, 70569 Stuttgart, Germany*
[3] *Pearlstone Center for Aeronautical Engineering Studies, Mechanical Engineering Department, Ben-Gurion University of the Negev, Beer-Sheva, Israel*

SUMMARY

The displacements of three-dimensional linearly elastic plate domains can be expanded as a compound power-series asymptotics, when the thickness parameter ε tends to zero. The leading term $\mathbf{u}^0$ in this expansion is the well-known Kirchhoff–Love displacement field, which is the solution to the limit case when $\varepsilon \to 0$. Herein, we focus our discussion on plate domains with either clamped or free lateral boundary conditions, and characterize the loading conditions for which the leading term vanishes. In these situations the first non-zero term $\mathbf{u}^k$ in the expansion appears for $k = 2, 3$ or 4 and is denoted as higher-order response of order 2, 3 or 4, respectively. We provide herein explicit loading conditions under which higher order responses in three-dimensional plate structures are visible, and demonstrate the mathematical analysis by numerical simulation using the *p*-version finite element method. Owing to the need for highly accurate results and 'needle elements' (having extremely large aspect ratio up to 10 000), a *p*-version finite element analysis is mandatory for obtaining reliable and highly accurate results. Copyright © 2001 John Wiley & Sons, Ltd.

KEY WORDS: high-order response; thin plates; linear elasticity; boundary layer; *p*-version FEM

1. INTRODUCTION

Plate domains are three-dimensional structures with one of their dimensions, usually denoted by 'thickness' (2ε), much smaller compared to the other two dimensions. In the linear theory of elasticity, the displacements solution $\mathbf{u}$ is of interest and can be considered as a function of the co-ordinates $\mathbf{x}$ and of ε: $\mathbf{u} = \mathbf{u}(\mathbf{x}, \varepsilon)$. If the loadings behave uniformly with respect to ε, see (3) and (4) later, it is natural to expand $\mathbf{u}(\mathbf{x}, \varepsilon)$ as an asymptotic series in ε. It is now

*Correspondence to: Zohar Yosibash, Mechanical Engineering Department, Ben-Gurion University of the Negev, P.O. Box 653, Beer-Sheva 84105, Israel
†E-mail: zohary@pversion.bgu.ac.il

Received 10 March 2000
Revised 28 February 2001

well understood that this problem has a singular perturbation nature as $\varepsilon \to 0$ giving rise to boundary layer effects, and that such an expansion can be provided in the general form, see also References [1–3],

$$\mathbf{u}(\mathbf{x},\varepsilon) \simeq \mathbf{u}^0\left(\mathbf{x},\frac{\mathbf{x}}{\varepsilon}\right)+\varepsilon\mathbf{u}^1\left(\mathbf{x},\frac{\mathbf{x}}{\varepsilon}\right)+\varepsilon^2\mathbf{u}^2\left(\mathbf{x},\frac{\mathbf{x}}{\varepsilon}\right)+\cdots+\varepsilon^k\mathbf{u}^k\left(\mathbf{x},\frac{\mathbf{x}}{\varepsilon}\right)\cdots \tag{1}$$

where $\mathbf{u}^0,\mathbf{u}^1,\ldots,\mathbf{u}^k$ are functions of the co-ordinates x_1,x_2 and x_3/ε. Detailed mathematical analysis on the asymptotics in thin isotropic plates, (see References [4–6] for clamped plates and Reference [7] for other lateral boundary conditions) makes it possible to explicitly quantify the various terms in expansion (1). Moreover, numerical realization of several terms in (1) has been presented in Reference [8].

Herein, we address plates with either *hard-clamped* or *free* lateral boundary conditions, and based on the mathematical analysis in References [9, 10] we present explicitly expressions for loading conditions for which the leading term $\mathbf{u}^0$ vanishes in expansion (1), providing a displacement field with a first non-vanishing term which is not $\mathbf{u}^1$ (that is zero too) but $\mathbf{u}^2$ (or even $\mathbf{u}^3$ or $\mathbf{u}^4$) denoted as higher-order response of order 2 (resp. 3 or 4). In these situations it may happen that a boundary layer term of the *same* order as the actual leading term appears in the displacement field. It is important to realize that there are loading conditions (which will be explicitly given herein) under which the Kirchhoff–Love solution of a three-dimensional plate vanish.

As to the practical engineering point of view, typical loadings where higher-order responses are excited may be very rare. A clamped thin plate on an airplane or a thin spoiler on a car subjected to pressure on top and bottom and with body forces due to gravitation, all having specific magnitudes, might be one such example. Beyond the engineering applicability in daily use of the presented results, the specific loading conditions explicitly provided herein, exciting higher-order responses, are of relevance from the computational point of view. These could serve as benchmarks for numerical codes simulating the response in thin elastic structures.

In the same spirit of Reference [8] (where we presented visualization of boundary layers in thin plates under 'usual loadings'), we herein visualize these higher-order responses using the p-version of the finite element method (FEM). Two of the major advantages of the p-FEM over traditional h-FEM are crucial for conducting this kind of analysis—namely: the possibility of using extremely large element aspect ratios (ratio between larger and smaller sides of an element) without deterioration of the numerical results, and exponential convergence rates, assuring high accuracy and reliability of the computed data.

This paper is organized as follows: In Section 2 we provide the necessary notations and preliminaries followed by explicit details on the three-dimensional solution for clamped and free plates. In Section 3 the general necessary and sufficient conditions on the loadings to provide higher-order responses are summarized, and explicit loading examples are provided which exhibit these higher-order responses. Numerical examples for demonstrating and visualizing higher-order responses, predicted by the mathematical analysis, are provided in Section 4. These numerical solutions are obtained by the p-version finite element method. We conclude in Section 5. An appendix with some of the formulae used in the paper is provided at the end.

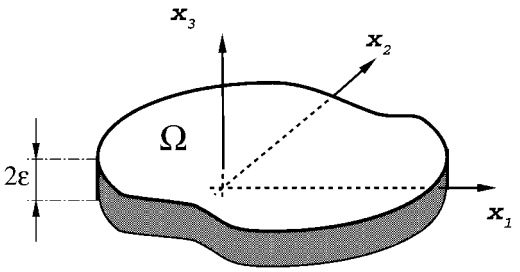

Figure 1. Typical plate of interest and notations.

2. NOTATIONS AND PRELIMINARIES

2.1. The elasticity problem

We consider a thin elastic, isotropic and homogeneous three-dimensional domain Ω defined as follows:

$$\Omega = \omega \times (-\varepsilon, +\varepsilon) \quad \text{with } \omega \subset \mathbb{R}^2 \text{ a regular domain}$$

and associated Cartesian co-ordinates are $\mathbf{x} = (x_1, x_2, x_3)$, see Figure 1. Let $(u_1, u_2, u_3)^{\mathrm{T}}$ denote the components of the displacement and let $\mathbf{e}$ denote the linearized strain tensor $e_{ij} = \frac{1}{2}(\partial_i u_j + \partial_j u_i)$, where $\partial_i \equiv \partial/\partial x_i$. The stress tensor $\boldsymbol{\sigma}$ is given by Hooke's law $\boldsymbol{\sigma} = [A]\mathbf{e}$, where $[A] = (A_{ijkl})$ is the compliance tensor of an isotropic material expressed in terms of the Lamé constants λ and μ:

$$A_{ijkl} = \lambda \delta_{ij}\delta_{kl} + \mu(\delta_{ik}\delta_{jl} + \delta_{il}\delta_{jk})$$

In the sequel, we will use either the Lamé constants or the equivalent engineering material coefficients:

$$\text{Young modulus } E = \frac{\mu(3\lambda + 2\mu)}{\lambda + \mu} \quad \text{and} \quad \text{Poisson ratio } \nu = \frac{\lambda}{2(\lambda + \mu)}$$

The tractions (surface forces) are denoted by $\mathbf{t} = \boldsymbol{\sigma} \cdot \mathbf{n}$, where $\mathbf{n}$ is the outward normal vector on the domain's boundary. We consider herein either clamped ($\mathbf{u} = \mathbf{0}$), or free ($\mathbf{t} = \mathbf{0}$) boundary conditions on the lateral face of the plate

$$\partial\Omega_L = \partial\omega \times (-\varepsilon, +\varepsilon)$$

The tractions on the upper face of the plate ($\Gamma^+ = \{\mathbf{x} \mid x_3 = \varepsilon\}$) and the corresponding lower face of the plate ($\Gamma^- = \{\mathbf{x} \mid x_3 = -\varepsilon\}$) are denoted by $\mathbf{t}^+$ (corr. $\mathbf{t}^-$). The volume forces are denoted by $\mathbf{f}$.

With above notation, we may state the weak formulation of the elasticity problem for the free plate

$$\text{Seek} \quad \mathbf{u} \in H^1(\Omega)^3 \quad \text{such that}$$

$$\int_\Omega [A]\mathbf{e}(\mathbf{u}) : \mathbf{e}(\mathbf{v}) = \int_\Omega \mathbf{f} \cdot \mathbf{v} + \int_{\Gamma^+} \mathbf{t}^+ \cdot \mathbf{v} + \int_{\Gamma^-} \mathbf{t}^- \cdot \mathbf{v}, \quad \forall \mathbf{v} \in H^1(\Omega)^3 \tag{2}$$

whereas for the clamped plate one simply needs to seek a solution in the space $[H^1_{\partial\Omega_L}]^3$, which are functions in $H^1(\Omega)^3$ with the additional constraint that $\mathbf{u}=\mathbf{0}$ on $\partial\Omega_L$.

Of course, in the case of free boundary conditions the applied tractions $\mathbf{t}^{\pm}$ and the volume forces $\mathbf{f}$ are supposed to be equilibrated versus the rigid displacements.

2.2. Scaled co-ordinates and assumptions on data

We denote by the Greek index α the in-plane variables $\{1,2\}$, by s a curvilinear co-ordinate along the lateral boundary of the plate ($\partial\omega$) and by n the distance to $\partial\omega$. We also use the subscripts $_n$ and $_s$ for the normal and tangential components of a field on the boundary $\partial\omega$.

The subscript $_*$ is used as condensed notation of in-plane variables. Thus we denote: $\mathbf{x}_* \stackrel{\text{def}}{=} (x_1, x_2)$, $\mathbf{u}_* \stackrel{\text{def}}{=} (u_1,u_2)^{\mathrm{T}}$, $\mathrm{div}_*\mathbf{u}_* \stackrel{\text{def}}{=} \partial_1 u_1+\partial_2 u_2$, $\nabla_* = (\partial_1,\partial_2)^{\mathrm{T}}$ and $\Delta_* \stackrel{\text{def}}{=} \partial_{11}+\partial_{22}$.

It is convenient to represent all quantities of an asymptotic expansion in a fixed reference domain, thus we stretch the plate along the vertical axis and define the stretched transverse variable

$$X_3 \stackrel{\text{def}}{=} x_3/\varepsilon$$

Moreover, a correct description of the boundary layer terms requires the introduction of the stretched distance to $\partial\omega$:

$$N \stackrel{\text{def}}{=} n/\varepsilon$$

In such an asymptotic analysis, it is natural to assume that the volume forces behave as fixed profiles in the scaled vertical variable X_3, compare with the reference work [11]. Moreover, like in the previous works [9, 10, 7], we suppose that they are of order of ε in the vertical direction, and of order $\mathcal{O}(1)$ in the in-plane directions, namely

$$f_\alpha(\mathbf{x}) = F_\alpha(x_1,x_2,X_3), \quad f_3(\mathbf{x}) = \varepsilon F_3(x_1,x_2,X_3) \tag{3}$$

with the data $\mathbf{F}=(F_1,F_2,F_3)^{\mathrm{T}}$ regular up to the boundary, i.e. $\mathbf{F}\in C^\infty(\bar{\omega}\times[-1,1])^3$. Correspondingly we assume for the tractions on the upper and lower faces of the plate:

$$t^{\pm}_\alpha(\mathbf{x}) = \varepsilon T^{\pm}_\alpha(x_1,x_2,X_3=\pm 1), \quad t_3(\mathbf{x}) = \varepsilon^2 T^{\pm}_3(x_1,x_2,X_3=\pm 1) \tag{4}$$

The above assumptions are the correct ones so that the *scaled* displacement $U(x_1,x_2,X_3)$ defined as $(\mathbf{u}_*,\varepsilon u_3)(\mathbf{x})$ has a limit (which is generically non-zero) as $\varepsilon\to 0$. Capital letters are usually used in the sequel to represent quantities independent of ε.

Note that, as we are in the framework of linearized elasticity, by superposition we can construct displacement asymptotics for any volume forces $\mathbf{f}(\mathbf{x},\varepsilon)$ and tractions $\mathbf{t}^{\pm}(\mathbf{x},\varepsilon)$ which can be expanded as power series of ε.

2.3. The three-dimensional solution

In this subsection we provide expressions for the displacements in terms of in-plane functions (functions based on the variables x_1,x_2), ε and loading conditions. The mathematical rigorous proofs for the following representation are provided in Reference [7] in a general setting, whereas herein we summarize the essential and provide explicit representation for a restricted class of cases. Due to the symmetry properties of isotropic plates, it is well known that

the displacements $\mathbf{u}$ can be split into a bending part and a membrane (or stretching) part according to

$$u_{\mathrm{b},\alpha}(x_3)=\tfrac{1}{2}(u_\alpha(x_3)-u_\alpha(-x_3)),\quad u_{\mathrm{b},3}(x_3)=\tfrac{1}{2}(u_3(x_3)+u_3(-x_3))$$

$$u_{\mathrm{m},\alpha}(x_3)=\tfrac{1}{2}(u_\alpha(x_3)+u_\alpha(-x_3)),\quad u_{\mathrm{m},3}(x_3)=\tfrac{1}{2}(u_3(x_3)-u_3(-x_3))$$

$\mathbf{u}_\mathrm{b}$ is the solution of (2) corresponding to the bending parts of the volume forces $\mathbf{f}_\mathrm{b}$ and tractions $\mathbf{t}_\mathrm{b}$, and similarly for the membrane.

We are going to describe now (see also the presentation in Reference [8]), the asymptotic expansion of $\mathbf{u}(\mathbf{x},\varepsilon)$ under assumptions (3) and (4). This expansion involves three sorts of terms:

(i) Kirchhoff–Love displacements,
(ii) Displacements $\mathbf{v}=\mathbf{v}(\mathbf{x}_*,X_3)$ with zero integral mean value

$$\forall\mathbf{x}_*\in\bar{\omega}\int_{-1}^{+1}\mathbf{v}(\mathbf{x}_*,X_3)\,\mathrm{d}X_3=0$$

(iii) Boundary layer terms $\boldsymbol{\varphi}=\boldsymbol{\varphi}(s,N,X_3)$ exponentially decreasing as $N\to\infty$.

The Kirchhoff–Love displacements are expressed by *generator functions* $\boldsymbol{\zeta}$ with three components $(\zeta_1,\zeta_2,\zeta_3)^\mathrm{T}(\mathbf{x}_*)$ *only depending on in-plane variables*, namely the membrane ones are generated by $\boldsymbol{\zeta}_*=(\zeta_1,\zeta_2)$ and the bending ones by ζ_3. We denote

$$U_\mathrm{m}^\mathrm{KL}(\boldsymbol{\zeta}_*)(\mathbf{x})\overset{\mathrm{def}}{=}(\zeta_1(\mathbf{x}_*),\zeta_2(\mathbf{x}_*),0) \tag{5}$$

$$U_\mathrm{b}^\mathrm{KL}(\zeta_3)(\mathbf{x})\overset{\mathrm{def}}{=}\left(-X_3\partial_1\zeta_3(\mathbf{x}_*),-X_3\partial_2\zeta_3(\mathbf{x}_*),\frac{1}{\varepsilon}\zeta_3(\mathbf{x}_*)\right)$$

$$=\frac{1}{\varepsilon}(-x_3\partial_1\zeta_3(\mathbf{x}_*),-x_3\partial_2\zeta_3(\mathbf{x}_*),\zeta_3(\mathbf{x}_*)) \tag{6}$$

Though containing ε, definition (6) reveals to be a most convenient one. We denote in a natural way

$$U^\mathrm{KL}(\boldsymbol{\zeta})\overset{\mathrm{def}}{=}U_\mathrm{m}^\mathrm{KL}(\boldsymbol{\zeta}_*)+U_\mathrm{b}^\mathrm{KL}(\zeta_3)$$

Under assumptions (3) and (4), the displacement solution of (2) can be expanded as

$$\mathbf{u}\simeq U^\mathrm{KL}(\boldsymbol{\zeta}^0)+\varepsilon(U^\mathrm{KL}(\boldsymbol{\zeta}^1)+\mathbf{v}^1+\boldsymbol{\varphi}^1)+\cdots+\varepsilon^k(U^\mathrm{KL}(\boldsymbol{\zeta}^k)+\mathbf{v}^k+\boldsymbol{\varphi}^k)\cdots \tag{7}$$

Remark. Compared to the general expansion (1), we see that $\mathbf{u}^0$ can be identified to $U^\mathrm{KL}(\boldsymbol{\zeta}^0)$, and for any $k\geqslant 1,\mathbf{u}^k$ is identified to the sum $U^\mathrm{KL}(\boldsymbol{\zeta}^k)+\mathbf{v}^k+\boldsymbol{\varphi}^k$.

Thus the expansions of the bending and membrane parts are

$$\mathbf{u}_\mathrm{b}\simeq U_\mathrm{b}^\mathrm{KL}(\zeta_3^0)+\varepsilon(U_\mathrm{b}^\mathrm{KL}(\zeta_3^1)+\mathbf{v}_\mathrm{b}^1+\boldsymbol{\varphi}_\mathrm{b}^1)+\varepsilon^2(U_\mathrm{b}^\mathrm{KL}(\zeta_3^2)+\mathbf{v}_\mathrm{b}^2+\boldsymbol{\varphi}_\mathrm{b}^2)+\cdots \tag{8}$$

$$\mathbf{u}_\mathrm{m}\simeq U_\mathrm{m}^\mathrm{KL}(\boldsymbol{\zeta}_*^0)+\varepsilon(U_\mathrm{m}^\mathrm{KL}(\boldsymbol{\zeta}_*^1)+\mathbf{v}_\mathrm{m}^1+\boldsymbol{\varphi}_\mathrm{m}^1)+\varepsilon^2(U_\mathrm{m}^\mathrm{KL}(\boldsymbol{\zeta}_*^2)+\mathbf{v}_\mathrm{m}^2+\boldsymbol{\varphi}_\mathrm{m}^2)+\cdots \tag{9}$$

Remark. The displacements $\mathbf{v}^1$ with zero integral mean value in (8) and (9) are

$$\mathbf{v}^1_{\mathrm{b}}(\mathbf{x}_*, X_3) = \frac{\nu}{6(1-\nu)}(0, 0, (3X_3^2 - 1)\,\Delta_*\zeta^0_3)^{\mathrm{T}} \tag{10}$$

$$\mathbf{v}^1_{\mathrm{m}}(\mathbf{x}_*, X_3) = \frac{\nu}{1-\nu}(0, 0, -X_3\,\mathrm{div}_*\,\boldsymbol{\zeta}^0_*)^{\mathrm{T}} \tag{11}$$

They are in fact completely determined by $\boldsymbol{\zeta}^0$.

Using (5), (6) and (10), (11), we can represent the leading terms modulo $\mathcal{O}(\varepsilon^2)$ in expansion (8) and (9) as follows:

$$\mathbf{u}_{\mathrm{b}} = \begin{pmatrix} -X_3\partial_1\zeta^0_3 & - & \varepsilon X_3\partial_1\zeta^1_3 & + & 0 & + & 0 \\ -X_3\partial_2\zeta^0_3 & - & \varepsilon X_3\partial_2\zeta^1_3 & + & 0 & + & 0 \\ \dfrac{1}{\varepsilon}\zeta^0_3 & + & \zeta^1_3 & + & \varepsilon\zeta^2_3 & + & \varepsilon\dfrac{\nu}{6(1-\nu)}(3X_3^2-1)\,\Delta_*\zeta^0_3 \end{pmatrix} + \varepsilon\boldsymbol{\varphi}^1_{\mathrm{b}} + \mathcal{O}(\varepsilon^2) \tag{12}$$

$$\mathbf{u}_{\mathrm{m}} = \begin{pmatrix} \zeta^0_1 & + & \varepsilon\zeta^1_1 & + & 0 \\ \zeta^0_2 & + & \varepsilon\zeta^1_2 & + & 0 \\ 0 & + & 0 & - & \varepsilon\dfrac{\nu}{1-\nu}X_3\,\mathrm{div}_*\,\boldsymbol{\zeta}^0_* \end{pmatrix} + \varepsilon\boldsymbol{\varphi}^1_{\mathrm{m}} + \mathcal{O}(\varepsilon^2) \tag{13}$$

where the symbol $\mathcal{O}(\varepsilon^2)$ means that the remainder is uniformly bounded by $c\,\varepsilon^2$, c being independent of ε.

Remark. In the hard-clamped case the first membrane boundary-layer term $\boldsymbol{\varphi}^1_{\mathrm{m}}$ (resp. bending $\boldsymbol{\varphi}^1_{\mathrm{b}}$), is only present if $\mathrm{div}_*\,\boldsymbol{\zeta}^0_*$ is non-zero on $\partial\omega$ (resp. $\Delta_*\zeta^0_3 \neq 0$ on $\partial\omega$). In the free situation $\boldsymbol{\varphi}^1 \equiv \boldsymbol{\varphi}^1_{\mathrm{b}}$ and $\boldsymbol{\varphi}^1$ is present only if $(\partial_n + \kappa)\partial_s\zeta^0_3$ is non-zero on $\partial\omega$, with κ denoting the curvature of $\partial\omega$. Visualization of these profiles is provided in Reference [8].

2.4. Membrane and bending equations for the generators

As shown in the previous subsection, the displacements can be expressed in term of in plane functions, $\boldsymbol{\zeta}^k$, called generators. The generator functions $\boldsymbol{\zeta}^k_*$ and ζ^k_3 are defined on ω and they are solutions to the following problems. $\boldsymbol{\zeta}^k_*$ is solution of the 'membrane equation'

$$\mu\Delta_*\boldsymbol{\zeta}^k_* + (\tilde{\lambda}+\mu)\nabla_*\,\mathrm{div}_*\,\boldsymbol{\zeta}^k_* = \mathbf{R}^k_{\mathrm{m}} \tag{14}$$

whereas ζ^k_3 solves the 'bending equation'

$$(\tilde{\lambda}+2\mu)\Delta_*^2\zeta^k_3 = R^k_{\mathrm{b}} \tag{15}$$

with $\tilde{\lambda} = 2\lambda\mu(\lambda+2\mu)^{-1}$. The right-hand sides $\mathbf{R}^k_{\mathrm{m}}$ and R^k_{b} depend on the data $\mathbf{F}$ and $\mathbf{T}^{\pm}$, and *only on* $\mathbf{x}_*$ *and not on* ε.

The right-hand side of (14) for $\boldsymbol{\zeta}_*^0$ is given by

$$\mathbf{R}_{\mathrm{m}}^0(\mathbf{x}_*) = -\frac{1}{2}\left[\int_{-1}^{+1} \mathbf{F}_*(\mathbf{x}_*, X_3)\,\mathrm{d}X_3 + \mathbf{T}_*^+ + \mathbf{T}_*^-\right]$$

and the right-hand side of (15) for ζ_3^0 is:

$$R_{\mathrm{b}}^0(\mathbf{x}_*) = \frac{3}{2}\left[\int_{-1}^{+1} F_3\,\mathrm{d}X_3 + T_3^+ + T_3^- + \mathrm{div}_*\left(\int_{-1}^{+1} X_3\,\mathbf{F}_*\,\mathrm{d}X_3 + \mathbf{T}_*^+ - \mathbf{T}_*^-\right)\right]$$

For $k=1$, we have simply $\mathbf{R}_{\mathrm{m}}^1 = 0$ and $R_{\mathrm{b}}^1 = 0$, whereas for $k=2$ formulas are much more involved and require the introduction of several new notations. For the sake of completeness, we simply quote them from Reference [9] in the appendix.

2.5. *Boundary conditions for the generators*

The boundary conditions for the generators on $\partial\omega$ depend of course on the specified boundary conditions on the lateral face of the plate.

(i) *For the hard clamped plate*: The boundary operators are the Dirichlet conditions associated with the membrane and bending operators in (14) and (15). For $k=0$ and 1, the boundary conditions are
$\zeta_3^0 = 0$, $\partial_n \zeta_3^0 = 0$ for the bending equation and $\boldsymbol{\zeta}_*^0 = \mathbf{0}$ for the membrane equation.
$\zeta_n^1 = c_1\,\mathrm{div}_*\boldsymbol{\zeta}_*^0$, $\zeta_s^1 = 0$, for the membrane equation and $\zeta_3^1 = 0$, $\partial_n\zeta_3^1 = c_2\,\Delta_*\zeta_3^0$, for the bending equation, where $c_1 = c_1(\lambda,\mu)$ and $c_2 = c_2(\lambda,\mu)$ are non-zero universal coefficients.

(ii) *For the free plate*: The boundary operators are the Neumann conditions associated with the correct bilinear forms corresponding to the membrane and bending operators in (14) and (15).

For $k=0$ these are: for the membrane equation

$$\mu(\partial_s\zeta_n^0 + \partial_n\zeta_s^0 + 2\kappa\zeta_s^0) = 0 \tag{16}$$

$$\tilde{\lambda}\,\mathrm{div}_*\,\boldsymbol{\zeta}_*^0 + 2\mu\partial_n\zeta_n^0 = 0 \tag{17}$$

and for the bending equation

$$\tilde{\lambda}\Delta_*\zeta_3^0 + 2\mu\partial_{nn}\zeta_3^0 = 0 \tag{18}$$

$$(\tilde{\lambda}+2\mu)\partial_n\Delta_*\zeta_3^0 + 2\mu\partial_s(\partial_n+\kappa)\partial_s\zeta_3^0 = \frac{3}{2}\left[\int_{-1}^{+1} X_3F_n\,\mathrm{d}X_3 + T_n^+ - T_n^-\right] \tag{19}$$

The generating function $\boldsymbol{\zeta}_*^1$ satisfies homogeneous boundary conditions like $\boldsymbol{\zeta}_*^0$ in (16) and (17). Since Equation (14) for $\boldsymbol{\zeta}_*^1$ is also homogeneous, then $\boldsymbol{\zeta}_*^1$ is identically zero.

For the bending equation

$$\tilde{\lambda}\Delta_*\zeta_3^1 + 2\mu\partial_{nn}\zeta_3^1 = c_3\partial_s(\partial_n + \kappa)\partial_s\zeta_3^0 \tag{20}$$

$$(\tilde{\lambda} + 2\mu)\partial_n\Delta_*\zeta_3^1 + 2\mu\partial_s(\partial_n + \kappa)\partial_s\zeta_3^1 = d(s) \tag{21}$$

where $c_3 = c_3(\lambda, \mu)$ is a universal coefficient and $d(s)$ depends on special traces of ζ_3^0 as well as on F_n and $T_n^{\pm}$.

3. HIGHER-ORDER RESPONSES

Under special loading conditions, which will be described in the sequel, the leading term in expansion (7) vanish, i.e. the generator $\boldsymbol{\zeta}^0 \equiv \mathbf{0}$, providing a displacement field of higher order. We define the order of the response according to:

Definition 3.1. With assumptions (3) and (4) and if $\boldsymbol{\zeta}^0 \equiv \mathbf{0}$, we call *order of the response* the smallest integer k such that at least one of the three terms $\boldsymbol{\zeta}^k$, $\mathbf{v}^k$ or $\boldsymbol{\varphi}^k$ involved in expansion (7) is not zero.

Readers interested in more detailed proofs of the results stated herein are referred to Reference [12]. The displacement asymptotic expansion for hard clamped plates is first considered followed by free plate lateral boundary conditions. We also highlight the difference in the higher-order responses due to the different lateral boundary conditions.

The reader is referenced to the appendix for detailed definition of the symbols $\mathfrak{G}$, and $\mathfrak{H}$ appearing in the sequel, although these definitions are not essential for the understanding of higher-order responses. These symbols reflect displacement functions of the type $\mathbf{v}$, and are generated by operations on the loadings $(\mathbf{F}, \mathbf{T}^{\pm})$.

The symbols, $[F]_m$ in the sequel, is defined as following:

Definition 3.2. $[F]_m$ denotes the mth moment with respect to X_3 of F:

$$[F]_m = \int_{-1}^{+1} X_3^m F(\mathbf{x}_*, X_3)\,\mathrm{d}X_3$$

3.1. Hard clamped plates

From equations (14) and (15) for $\boldsymbol{\zeta}^0$ and the associated homogeneous boundary conditions, it is clear that if $\mathbf{R}_{\mathrm{m}}^0$ and R_{b}^0 are zero, then $\boldsymbol{\zeta}^0 \equiv \mathbf{0}$. In this case, as $\mathbf{R}_{\mathrm{m}}^1$ and R_{b}^1 are zero too and the boundary data of $\boldsymbol{\zeta}^1$ depends linearly on $\boldsymbol{\zeta}^0$, we also have $\boldsymbol{\zeta}^1 \equiv \mathbf{0}$. Formulas (10) and (11) yield that $\mathbf{v}^1 \equiv \mathbf{0}$. Moreover, as $\boldsymbol{\varphi}^1$ also depends linearly on $\boldsymbol{\zeta}^0$, it is zero too. Thus the order of the response is at least 2.

Theorem 3.3 ([9]). For any loading $(\mathbf{f}, \mathbf{t}^{\pm})$ such that $\mathbf{R}_{\mathrm{m}}^0 = \mathbf{0}$ and $R_{\mathrm{b}}^0 = 0$, and that either $\mathbf{R}_{\mathrm{m}}^2$ or R_{b}^2 or $\mathfrak{G}(\mathbf{F}, \mathbf{T}^{\pm})$ is not identically zero, the order of the response is 2. The first non-zero

term in expansion (7) of $\mathbf{u}$ is

$$\varepsilon^2 \left(U^{\mathrm{KL}}(\boldsymbol{\zeta}^2) + \underbrace{\mathfrak{G}_*(\mathbf{F}, \mathbf{T}^{\pm})}_{=\mathbf{v}^2} + \boldsymbol{\varphi}^2 \right) \tag{22}$$

As corollaries of Theorem 3.3 we exhibit special load conditions to excite order 2 responses in bending and membrane solutions.

Corollary 3.4 ([9]). Let $f_3 = t_3^{\pm} = 0$, $\mathbf{f}_* = -3X_3(1,1)^{\mathrm{T}}$, $\mathbf{t}_*^{+} = (\varepsilon, \varepsilon)^{\mathrm{T}}$ and $\mathbf{t}_*^{-} = -(\varepsilon, \varepsilon)^{\mathrm{T}}$ representing a bending load. Then we have an order 2 response and the expansion of the displacement $\mathbf{u} = \mathbf{u}_{\mathrm{b}}$ starts like

$$\mathbf{u}_{\mathrm{b}} = \varepsilon^2 \left[\begin{pmatrix} -X_3\partial_1\zeta_3^2 & + & 0 & + & \mathfrak{G}_1 \\ -X_3\partial_2\zeta_3^2 & + & 0 & + & \mathfrak{G}_2 \\ \frac{1}{\varepsilon}\zeta_3^2 & + & \zeta_3^3 & + & 0 \end{pmatrix} + \boldsymbol{\varphi}_{\mathrm{b}}^2 + \mathcal{O}(\varepsilon) \right] \tag{23}$$

with $\mathfrak{G}_1 = \mathfrak{G}_2 = (2\mu)^{-1}(X_3^3 - X_3)$.

Corollary 3.5 ([9]). Let $f_3 = t_3^{\pm} = 0$, $\mathbf{f}_* = -(1,1)^{\mathrm{T}}$, $\mathbf{t}_*^{\pm} = (\varepsilon, \varepsilon)^{\mathrm{T}}$ representing a membrane load. Then we have an order 2 response and the expansion of $\mathbf{u} = \mathbf{u}_{\mathrm{m}}$ starts like

$$\mathbf{u}_{\mathrm{m}} = \varepsilon^2 \left[\begin{pmatrix} \zeta_1^2 & + & \mathfrak{G}_1 \\ \zeta_2^2 & + & \mathfrak{G}_2 \\ & 0 & \end{pmatrix} + \boldsymbol{\varphi}_{\mathrm{m}}^2 + \mathcal{O}(\varepsilon) \right] \tag{24}$$

with $\mathfrak{G}_1 = \mathfrak{G}_2 = (3\mu)^{-1}(3X_3^2 - 1)$.

We may have higher orders than 2:

Theorem 3.6 ([9]). For any loading case which satisfies $(\mathbf{f}_*, \mathbf{t}_*^{\pm}) = \mathbf{0}$ and

$$([F_3]_0 + T_3^{+} + T_3^{-}) = \nabla_*([F_3]_1 + T_3^{+} - T_3^{-}) = \Delta_*([F_3]_2 - [F_3]_0) = 0 \quad \text{in } \omega$$

then $\mathbf{R}_{\mathrm{m}}^0 = \mathbf{R}_{\mathrm{m}}^2 = R_{\mathrm{b}}^0 = R_{\mathrm{b}}^2 = 0$ and $\mathfrak{G}(\mathbf{F}, \mathbf{T}^{\pm}) = \mathbf{0}$, and the order of the answer is $\geqslant 3$.

As corollaries of Theorem 3.6 we exhibit special load conditions to excite order 3 responses in bending and membrane solutions. Then first non-zero term in the expansion (7) of $\mathbf{u}$ is

$$\varepsilon^3 \left(U^{\mathrm{KL}}(\boldsymbol{\zeta}^3) + \underbrace{(\mathbf{0}, \mathfrak{H}_3(\mathbf{F}, \mathbf{T}^{\pm}))}_{=\mathbf{v}^3} + \boldsymbol{\varphi}^3 \right) \tag{25}$$

Corollary 3.7 ([9]). Let $f_3 = \varepsilon(X_3^2 - 1/3)$ and $t_3^{\pm} = 0$. Then we have an order 3 response and the expansion of the displacement $\mathbf{u} = \mathbf{u}_\mathrm{b}$ starts like

$$\mathbf{u}_\mathrm{b} = \varepsilon^3 \left[\begin{pmatrix} -X_3\partial_1\zeta_3^3 & + & 0 & + & 0 \\ -X_3\partial_2\zeta_3^3 & + & 0 & + & 0 \\ \frac{1}{\varepsilon}\zeta_3^3 & + & \zeta_3^4 & + & \mathfrak{H}_3 \end{pmatrix} + \boldsymbol{\varphi}_\mathrm{b}^3 + \mathcal{O}(\varepsilon) \right] \tag{26}$$

Here $\mathfrak{H}_3$ is a non-zero even polynomial of degree 4 in X_3.

Corollary 3.8. Let $f_3 = \varepsilon$, $t_3^{\pm} = -\varepsilon^2$. Then we have an order 3 response and the expansion of the displacement $\mathbf{u} = \mathbf{u}_\mathrm{b}$ starts like in (6).

Corollary 3.9 ([9]). Let $f_3 = 0$, $t_3^{+} = \varepsilon^2$ and $t_3^{-} = -\varepsilon^2$. Then we have an order 3 response and the expansion of the displacement $\mathbf{u} = \mathbf{u}_\mathrm{m}$ starts like

$$\mathbf{u}_\mathrm{m} = \varepsilon^3 \left[\begin{pmatrix} \zeta_1^3 & + & 0 \\ \zeta_2^3 & + & 0 \\ 0 & + & \mathfrak{H}_3 \end{pmatrix} + \boldsymbol{\varphi}_\mathrm{m}^2 + \mathcal{O}(\varepsilon) \right] \tag{27}$$

with $\mathfrak{H}_3 = (\lambda + 2\mu)^{-1} X_3$.

Remark. There exist loads $\mathbf{f}$ and $\mathbf{t}^{\pm}$ which may generate fourth-order response. Specific loadings for this case can be found in Reference [9]. But if the loads are not identically zero and satisfy (3) and (4), we cannot have order 5 responses or larger.

3.2. Free plates

Theorem 3.10 ([10]). For any loading $\mathbf{f}$ and $\mathbf{t}^{\pm}$ such that $\mathbf{R}_\mathrm{m}^0 = \mathbf{0}$, $R_\mathrm{b}^0 = 0$ in ω and $\frac{3}{2}[\int_{-1}^{+1} X_3 F_n \, \mathrm{d}X_3 + T_n^+ - T_n^-] = 0$ on $\partial\omega$, the order of the response is $\geqslant 2$. If either $\mathbf{R}_\mathrm{m}^2$ or R_b^2 or $\mathfrak{G}(\mathbf{F}, \mathbf{T}^{\pm})$ or one of the boundary conditions for $\boldsymbol{\zeta}^2$ is not identically zero, then the order of the response is 2 and the expansion of $\mathbf{u}$ starts like in (23) and (24).

Theorem 3.11 ([10]). The order of the response is $\geqslant 3$ if and only if the generators $\boldsymbol{\zeta}^k \equiv 0$, $k = 0, 1, 2$, and additionally $\mathfrak{G}(\mathbf{F}, \mathbf{T}^{\pm}) = \mathbf{0}$. This is exactly the case if $\mathbf{f}_* = \mathbf{t}_*^{\pm} = \mathbf{0}$ and

$$([F_3]_0 + T_3^+ + T_3^-) = ([F_3]_1 + T_3^+ - T_3^-) = ([F_3]_2 - [F_3]_0) = 0 \quad \text{in } \omega$$

Then the expansion of $\mathbf{u}$ starts like in (26) and (27).

Comparing Theorem 3.11 (for the free plate) with Theorem 3.6 (for the hard clamped plate) one notices that if a loading produces an order 3 response for the free plate then the same loading will produce a higher-order response for the hard clamped plate as well, but contrary there exist loadings which produce a higher-order response in the hard-clamped plate and does not produce it in the free plate, see Reference [12].

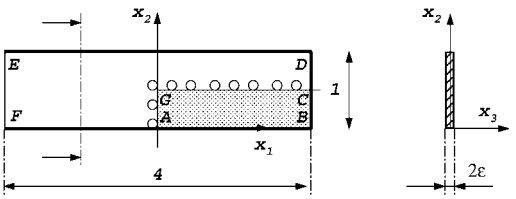

Figure 2. Rectangular plate under consideration.

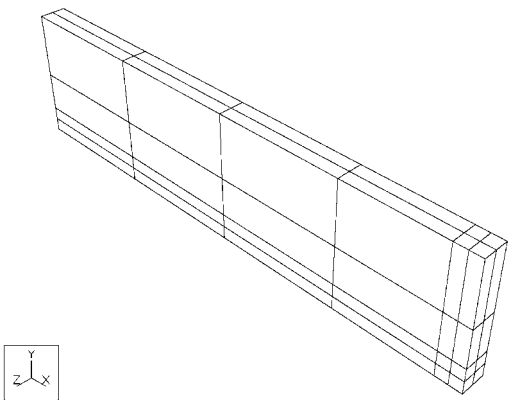

Figure 3. Finite element mesh for the plate with $2\varepsilon = 0.1$.

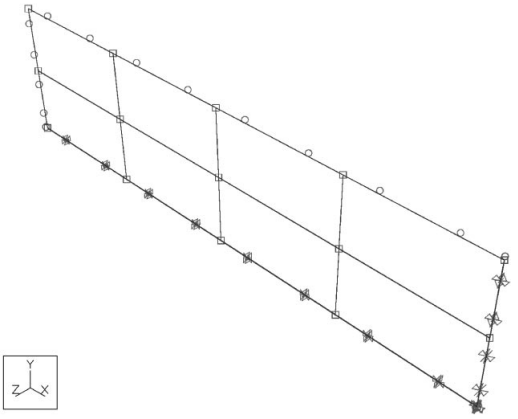

Figure 4. Finite element mesh and boundary conditions for the plate with $2\varepsilon = 0.001$.

4. NUMERICAL VISUALIZATION OF HIGHER-ORDER RESPONSES USING *p*-FEM

The theoretical results are visualized by computing functionals associated with the displacement field for free and hard clamped lateral boundary conditions, and for various loadings exciting the higher-order terms. The computations are done within the finite element code Stress Check.[‡] We consider a rectangular plate with dimensions $4 \times 1 \times 2\varepsilon$ as shown in Figure 2. The material properties are: Poisson ratio $\nu = 1/8$ and Young modulus $E = 27/4$. All lateral boundary conditions are either free or hard clamped, thus there are two axes of symmetry, so that only a quarter of the plate may be analysed, namely plate $ABCG$, with symmetry boundary conditions on AG and GC.

A three dimensional *p*-version finite element model is constructed having two elements in the thickness direction, four elements in the x_2 direction and six elements in the x_1 direction. In the neighbourhood of the edges, the mesh is graded so that there are two elements of dimension ε each. See Figure 3 for a typical mesh for $2\varepsilon = 0.1$ and Figure 4 for $2\varepsilon = 0.001$ and hard clamped lateral boundary conditions. The finite element model is constructed

[‡]Stress Check is a trade mark of Engineering Software Research and Development, Inc., 10845 Olive Blvd., Suite 170, St. Louis, MO 63141, USA.

parametrically so that the value of 2ε may vary, and we change it from 0.1 ($=10^{-1}$) to 0.001 ($=10^{-3}$). Although not visible in Figure 4, there are two elements across the thickness and two elements each of dimension ε in the neighbourhood of the boundary. The p-level over each element has been increased from 1 to 8 and the trunk space has been used (see Reference [13]). There are 12 568 degrees of freedom at $p=8$. An advantage of using p-version finite element methods is this possibility of having 'needle elements' in the boundary layer zone with aspect ratios as large as 10 000 without significant degradation in the numerical performance. An *exponential convergence rate* is obtained (due to the use of high-order elements) and the convergence of the computed data has been examined as well for increasing p-levels in order to evaluate the reliability of the numerical results.

By considering (8) and (9), one notices that in the generic case the displacement field is dominated by the Kirchhoff–Love components, in particular the transversal bending component of $U_{\mathrm{b}}^{\mathrm{KL}}(\zeta_3^0)$ is much larger than any other component of the displacement. In contrast to that, for the higher-order responses the operators $\mathfrak{G}$ and $\mathfrak{H}$ play an important role in the expansion of the displacement field, see (22)–(24) and (25)–(27). In order to be able to visualize single terms in the expansion for the considered examples and in particular to extract constants with respect to X_3 as well as expressions with vanishing integral mean value, we introduce for $j=1,2,3$ and $i,m\in\mathbb{N}$ the following quantities:

$$J_m[u_j,P_i]=\frac{1}{(2\varepsilon)^m}\int_{-1}^{+1}u_j(\mathbf{x}_*,X_3)P_i(X_3)\,\mathrm{d}X_3 \tag{28}$$

where P_i is the ith Legendre polynomial. Since $\boldsymbol{\zeta}^k$ are constants in X_3 then they are L_2-orthogonal to P_i ($i\neq 0$). In contrast to that, the expressions $\mathbf{v}^k$ are orthogonal to P_0. Based on the parity properties of the membrane and bending parts, the quantities $J_m[u_j,P_i]$ vanish either for all even or for all odd values of i depending on the type and on the component of the displacement field under consideration. The quantities in (28) will enable us to visualize in the higher-order response, the single parts in the leading terms and in particular to make the appearing boundary layer effects visible.

4.1. Hard clamped plate, bending response of order 3

The first example which we consider should be understood as a motivating example in order to indicate the existence of higher-order responses and their significance. The loadings for this example read: $f_\alpha=0,\ t_\alpha^\pm=0,\ f_3=\varepsilon,\ t_3^\pm=-\gamma\varepsilon^2$ with γ a real parameter. In the following we are going to change γ such that the existence of a higher-order response will be visible. For $\gamma=1$, the loading is as in Corollary 3.8, thus one expects u_3 to behave as ε^2 as $\varepsilon\to 0$. For any other $\gamma\neq 1$, the 'bending' solution, with the Kirchhoff–Love vertical component $u_3\to\infty$ like $1/\varepsilon$ is expected as $\varepsilon\to 0$.

To be able to obtain a global information about the behaviour of the displacement field we introduce a global L_2-norm (on the whole plate)

$$I(u_j)=\sqrt{\frac{1}{2\varepsilon}\int_\Omega |u_j|^2\,\mathrm{d}x_1\,\mathrm{d}x_2\,\mathrm{d}x_3} \tag{29}$$

We expect that for $\gamma\neq 1$ and for $\varepsilon\to 0, I(u_3)$ tends to infinity with an order $\mathcal{O}(\varepsilon^{-1})$ as predicted by (8), but for $\gamma=1$, $I(u_3)$ will converge to zero with an order $\mathcal{O}(\varepsilon^2)$. This should also have

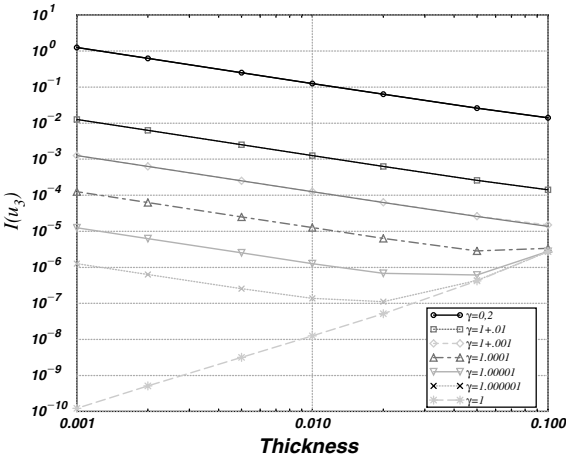

Figure 5. $I(u_3)$ for various γ as $2\varepsilon \to 0$.

some influence for γ close to one, but the change for $I(u_3)$ from tending to infinity with an order $\mathcal{O}(\varepsilon^{-1})$ to tending to zero with an order $\mathcal{O}(\varepsilon^2)$ should be smooth (with maybe high gradients) with respect to the change of γ near $\gamma = 1$. Indeed, as expected by the mathematical analysis, the numerical results obtained from the finite element solution, shown in Figure 5, demonstrate this behaviour.

4.2. *Hard clamped plate, bending response of order 2*

The second example which we consider is a bending example and the loadings are the following: $f_1 = f_2 = -3X_3,\ f_3 = 0,\ t_1^{\pm} = t_2^{\pm} = \pm\varepsilon,\ t_3^{\pm} = 0$. This loading according to Corollary 3.4 produces an order 2 response.

In Figure 6 we present the functional $J_2[u_3, P_2]$ along the line $x_1 = 1,\ 0 \leqslant x_2 \leqslant 0.15$, i.e. with respect to the *physical* distance to the lateral boundary. Since P_2 is orthogonal to the constant (over the thickness) terms ζ_3^k, we expect that $J_2[u_3, P_2]$ will vary in the boundary layer zone only due to the presence of the boundary layer term $\varphi_{\mathrm{b},3}^2$ in the leading term of the asymptotic expansion and then will vanish as we move inside the plate. We moreover expect to see how the width of the boundary layer varies in dependence of ε, since we have chosen a representation in the physical variable. It can be noticed that indeed the boundary layer is only active in a strip of a width of order ε in the vicinity of the lateral boundary.

However, such an evaluation does not allow a comparison of the single functionals $J_2[u_3, P_2]$ for different values of ε in the boundary layer zone. That is the reason why in the following the functionals $J_m[u_j, P_i]$ are always evaluated with respect to the stretched distance $x_2/2\varepsilon$. So we evaluate $J_m[u_j, P_i]$ on a set of equidistant points along the line $x_1 = 1,\ 0 \leqslant x_2/2\varepsilon \leqslant 3$. We notice in this case, as shown in Figure 7, that the curves for different values of ε overlap, i.e they are independent of ε. Moreover, $J_2[u_3, P_2]$ is almost zero for $x_2/2\varepsilon > 1$, which manifests a rapidly decreasing profile. All of this is in accordance with the prediction of the mathematical analysis.

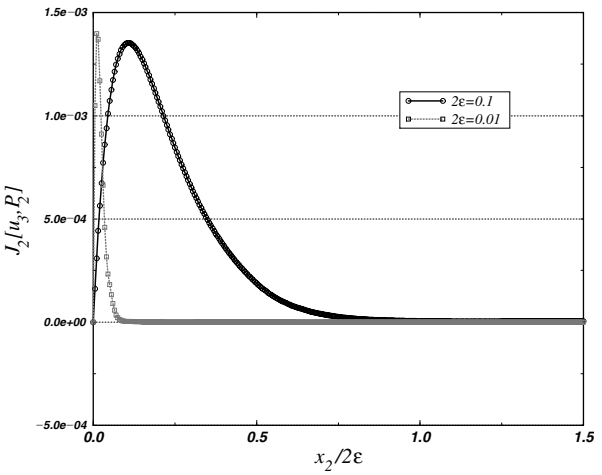

Figure 6. Hard clamped $J_2[u_3, P_2]$.

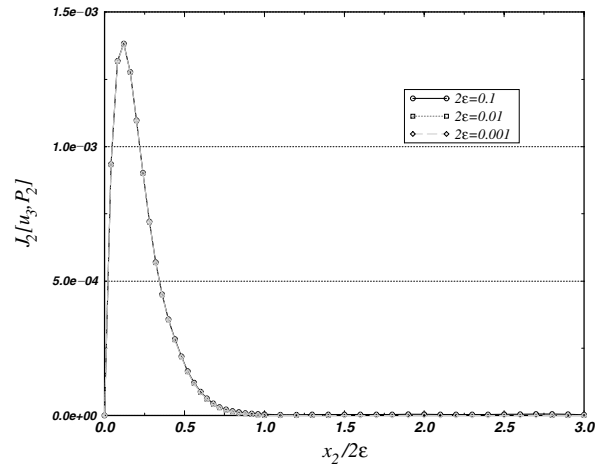

Figure 7. Hard clamped $J_2[u_3, P_2]$ vis. stretched distance.

In Figure 8 we present $J_1[u_3, P_0]$ with respect to the physical variable x_2. We expect to see ζ_3^2 only, since all the other terms are of higher order. Moreover, if we can see a boundary layer zone at all, it should be of width ε as in Figure 6. But as said above in order to be able to visualize the boundary layer behaviour we are interested in the evaluation with respect to the stretched variable $x_2/2\varepsilon$, which we present in Figure 9.

Since $J_2[u_3, P_0]$ is nothing but the integral mean value of u_3 across the thickness, we now expect to see the influence of both ζ_3^2 and $\varphi_{\mathrm{b},3}^2$. At the first look one would expect that because of the presence of ζ_3^2 in the asymptotic expansion $m = 1$ would hold and moreover, it would be $1/\varepsilon$ larger than $\varphi_{\mathrm{b},3}^2$. But as it can be seen from Figure 9 this is not true and $m = 2$ turns out to be the correct value. The reason for this is that we have evaluated $J_2[u_3, P_0]$ with

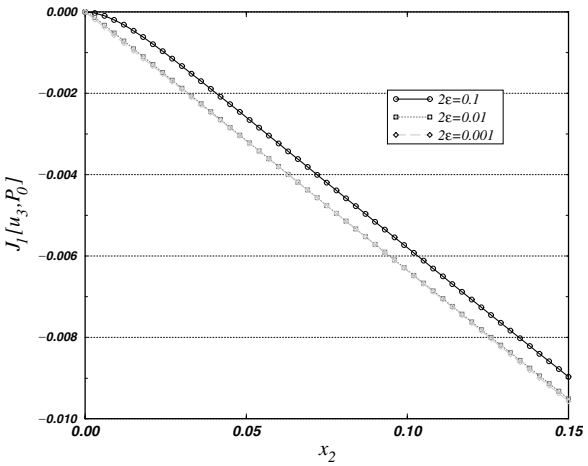

Figure 8. Hard clamped $J_1[u_3, P_0]$.

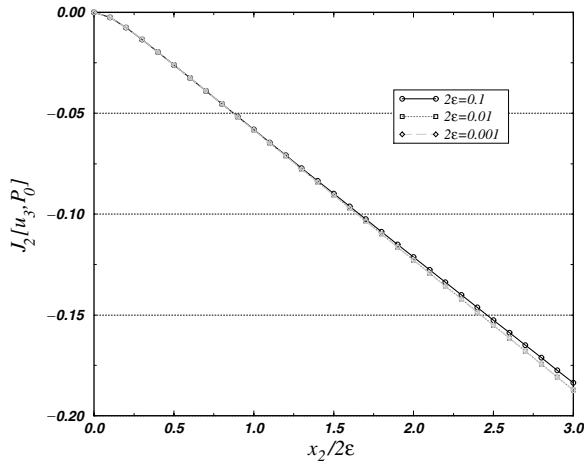

Figure 9. Hard clamped $J_2[u_3, P_0]$.

respect to the stretched variable $x_2/2\varepsilon$, while ζ_3^2 in fact depends on the physical distance x_2. But, if one develops ζ_3^2 in its Taylor series with respect to x_2 around $x_2 = 0$, then in this series the constant (in x_2) vanishes because of the lateral Dirichlet condition $\zeta_3^2 = 0$ on $\partial\omega$, and the Taylor series starts with a linear (in x_2) part. Considering now the Taylor series of ζ_3^2 with respect to the stretched variable $x_2/2\varepsilon$ (around $x_2 = 0$), i.e. we replace any x_2 in the series above by $\varepsilon(x_2/\varepsilon)$, it turns out that the asymptotic expansion of u_3 indeed starts with ε^2, such that $m = 2$ is the correct choice. In Figure 9 there is almost no boundary layer behaviour visible, which means that ζ_3^2 dominates $\varphi_{\mathrm{b},3}^2$.

In Figure 10 we visualize $J_2[u_1, P_1]$. We expect to see the influence of all the three terms $-X_3\partial_1\zeta_3^2$, $\mathfrak{G}_1$ and $\varphi_{\mathrm{b},1}^2$ which are contained in the leading term of the expansion. But in fact

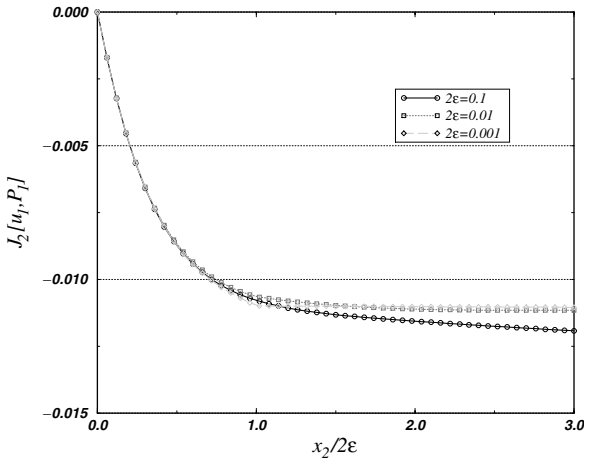

Figure 10. Hard clamped $J_2[u_1, P_1]$.

$J_2[u_1, P_1]$ varies in the boundary layer zone due to effect of the boundary layer profile $\varphi^2_{\mathrm{b},1}$ and becomes constant as we move away from the boundary inside the plate, which is the effect of $\mathfrak{G}_1$. Indeed, $J_2[u_1, P_1]$ tends to $-1/90$ in the interior of the plate which is the exact value of $J_2[\varepsilon^2\mathfrak{G}_1, P_1]$, i.e. $\varepsilon^2\mathfrak{G}_1$ represents the leading term in the expansion of u_1 outside the boundary layer zone. Here we recall that it holds $\mathfrak{G}_{\mathrm{b},\alpha} = (2\mu)^{-1}(X_3^3 - X_3)$, compare Corollary 3.4. The explanation why we cannot see $-X_3\partial_1\zeta_3^2$ is similar to the one in Figure 9. Since $x_1 \equiv s$ in the boundary layer zone, there $\partial_1\zeta_3^2$ coincides with $\partial_s\zeta_3^2$, which vanishes for $x_2 = 0$ because of the lateral Dirichlet condition $\zeta_3^2 = 0$ on $\partial\omega$. But this means that the Taylor series of $\partial_1\zeta_3^2$ in x_2 around $x_2 = 0$ starts with the linear term and hence the Taylor series in $x_2/2\varepsilon$ starts altogether with ε^3 and thus is in fact not present in the leading term.

In Figure 11, we present $J_2[u_2, P_1]$. In contrast to Figure 10, where we only saw $\mathfrak{G}_1$ and $\varphi^2_{\mathrm{b},1}$, here we really would expect to see the influence of all the three terms $-X_3\partial_2\zeta_3^2$, $\mathfrak{G}_2$ and $\varphi^2_{\mathrm{b},2}$ which build up the leading term of the expansion. The reason for this difference is that in the boundary layer zone $\partial_2\zeta_3^2$ coincides with $\partial_n\zeta_3^2$ due to the fact $x_2 \equiv n$ there. In contrast to $\partial_s\zeta_3^2$ in the previous graph, now $\partial_n\zeta_3^2$ is in general non-zero for $x_2 = 0$, compare Theorem 5.1 of Reference [9], so that its Taylor series with respect to x_2 around $x_2 = 0$ starts with the constant term and hence now should be visible in the graph. Indeed this fact can be stated in the figure. In the boundary layer zone we see $J_2[u_2, P_1]$ varying due to the effect of $\varphi^2_{\mathrm{b},2}$. Although $J_2[u_2, P_1]$ becomes more or less constant as we move inside the plate, this constant cannot be only the effect of $\mathfrak{G}_2$, since the value of the constant is approximately -0.0004 and not $-1/90$ as in the previous graph. This discrepancy is in fact produced by the presence of $-X_3\partial_n\zeta_3^2$ in the leading term, or better by the constant term of its Taylor series in x_2 in the same manner as it is explained above.

4.3. Hard clamped plate, membrane response of order 2

The next example is a membrane one with the loadings: $f_\alpha = -1$, $f_3 = 0$, $t_\alpha^\pm = \varepsilon$, $t_3^\pm = 0$, which in accordance with Corollary 3.5 produces an order 2 response.

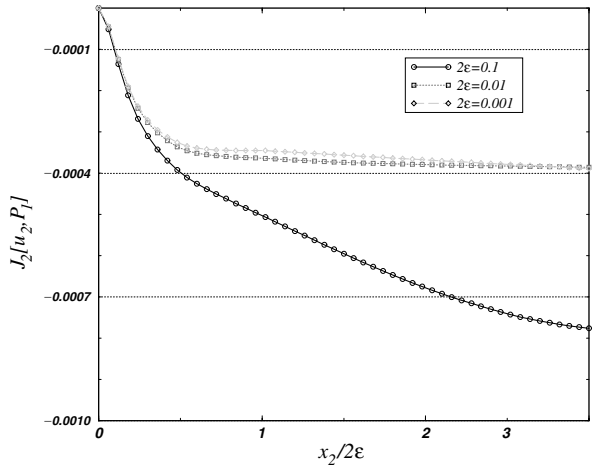

Figure 11. Hard clamped $J_2[u_2, P_1]$.

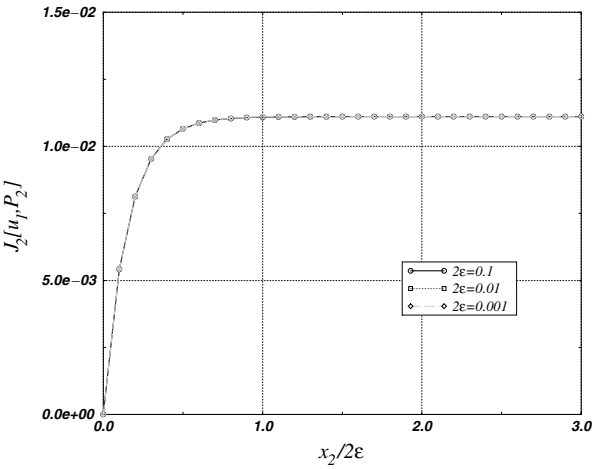

Figure 12. Hard clamped $J_2[u_1, P_2]$.

The values of the considered functionals are for $m = 2$ independent of ε which indicates that the asymptotic expansion starts in accordance with the analysis with ε^2. We first consider the first component of the displacement field u_1. The behaviour of the second component is very similar.

In Figure 12 we present $J_2[u_1, P_2]$. The graph shows clearly the existence of a boundary layer profile in the leading term of the expansion. This boundary layer profile is only present in a vicinity of the lateral boundary. Since in this case $\mathfrak{G}_1$ is simply a multiple of the Legendre polynomial P_2 (cf. Corollary 3.5), and ζ_1^2 is of course a constant in X_3, $J_2[u_1, P_2]$ tends to a constant as we move away from the boundary, representing the presence of $\mathfrak{G}_1$.

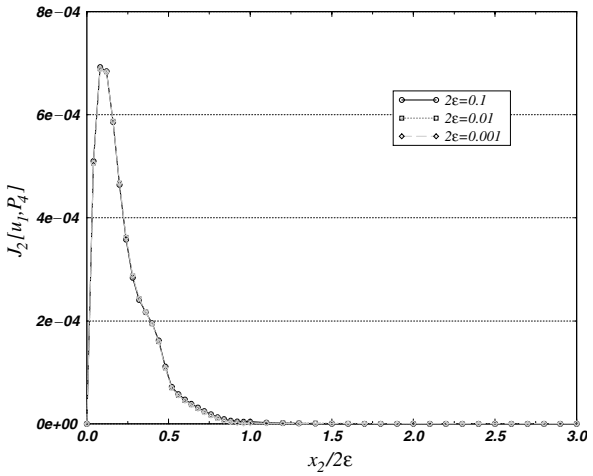

Figure 13. Hard clamped $J_2[u_1, P_4]$.

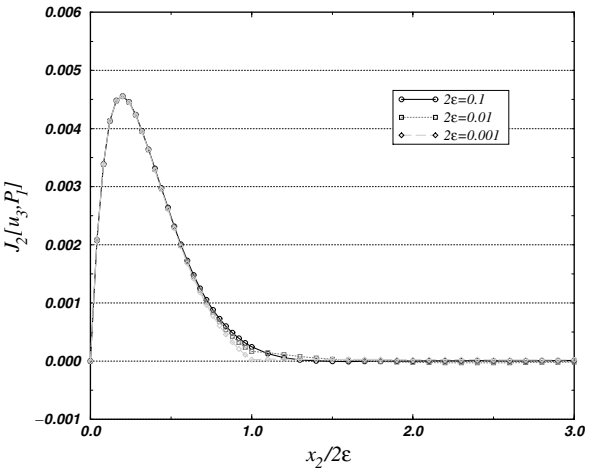

Figure 14. Hard clamped $J_2[u_3, P_1]$.

In Figure 13 $J_2[u_1, P_4]$ shows, as in the preceding graph, a boundary layer behaviour in a vicinity of the lateral boundary but then in contrast to it becomes zero outside the boundary layer, since as said above $\mathfrak{G}_1$ is a multiple of P_2 and hence orthogonal to P_4.

In Figure 14 we visualize with the help of $J_2[u_3, P_1]$ the behaviour of the third component of the displacement field u_3. We see a boundary layer behaviour in a neighbourhood of the lateral boundary and then the considered functional tends to zero as we move away from the boundary. The same behaviour is visible for $J_2[u_3, P_3]$ (not presented herein).

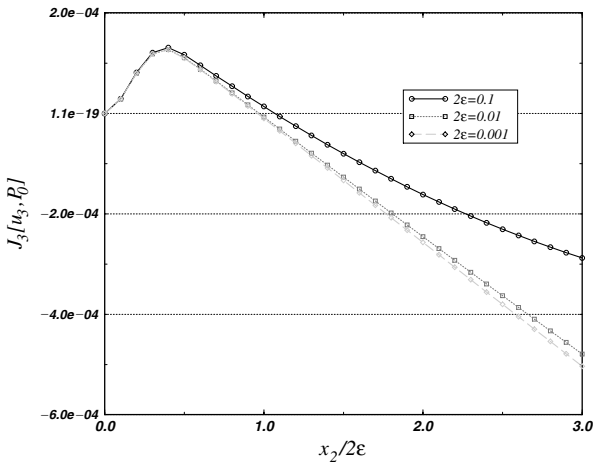

Figure 15. Hard clamped $J_3[u_3, P_0]$.

4.4. *Hard clamped vis free lateral boundary conditions*

The last example which we investigate shows the influence of the lateral boundary conditions on the higher-order responses. We consider the following bending loadings: $f_\alpha = 0$, $f_3 = \varepsilon(X_3^2 - \frac{1}{3})$, $\mathbf{t}^{\pm} = 0$. In accordance with Corollary 3.7 this loading produces an order 3 response in the hard clamped plate, but according to Theorems 3.10 and 3.11 only an order 2 response in the free plate.

In Figure 15 one notices the behaviour of $J_3[u_3, P_0]$ in the hard clamped case. Convergence for $m = 3$ is noticed (and small values of ε, which is not that fast as $\varepsilon \to 0$) although $m = 2$ would be the correct value predicted by the analysis. But this can be explained analogously to Figure 9 by the Taylor expansion of ζ_3^3 with respect to x_2 around $x_2 = 0$ and the fact that due to the boundary condition $\zeta_3^3 = 0$ on $\partial\omega$, this Taylor series starts with the linear term and hence altogether in x_2/ε with ε^3.

For the free lateral boundary conditions we first consider the behaviour of $J_1[u_3, P_0]$ as shown in Figure 16. As predicted by the analysis here $m = 1$ is the right choice. In contrast to the hard clamped situation now the constant part of the Taylor series of ζ_3^2 with respect to x_2 around $x_2 = 0$ is present and non-zero for free lateral boundary conditions. In comparison with the preceding graph now the dramatic influence of the lateral boundary condition on the higher-order response is visible which manifests itself in the discrepancy of the values of m in the considered lateral boundary conditions ($m = 1$ in the free and $m = 3$ in the hard clamped case). We emphasize that although the same loading is considered in both cases of lateral boundary conditions, the asymptotic expansion in the hard clamped case starts with two powers of ε later than in the free one.

Actually, the discrepancy of the ε-powers in the asymptotic expansions is indeed only one power of ε, since one more ε-power is due to the different behaviour of the Taylor series of the leading generators in the two different cases of boundary conditions. This different behaviour is due to the fact that we evaluate the functionals with respect to the scaled variable x_2/ε although in reality the leading generators in the expansion depend on the physical variable x_2. That this is indeed the explanation can be seen easily by first subtracting from $J_1[u_3, P_0]$

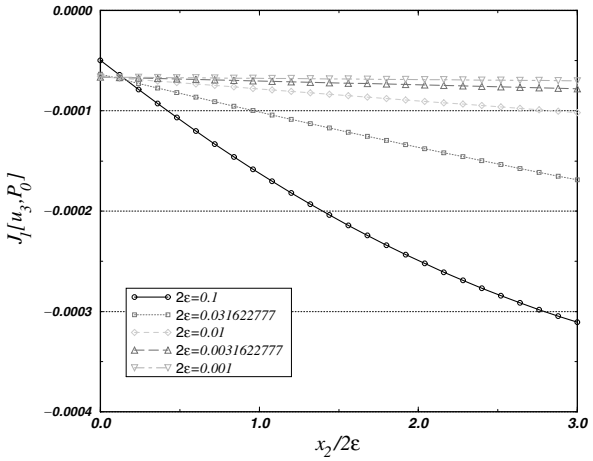

Figure 16. Free $J_1[u_3, P_0]$.

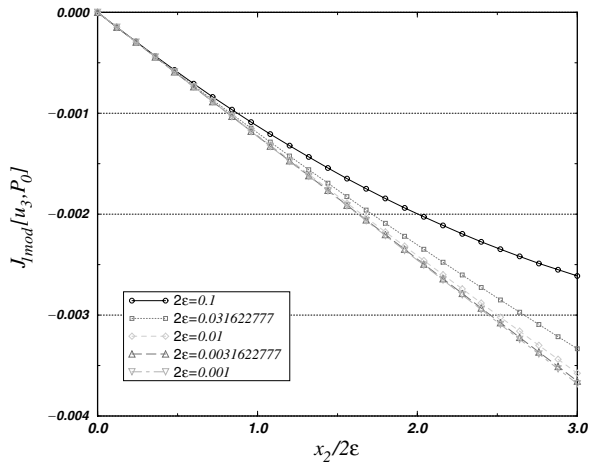

Figure 17. Free $[J_1[u_3, P_0] - J_1[u_3, P_0]_{x_2=0}]/(2\varepsilon)$.

its limit value for $x_2 = 0$ and then dividing the result once more by ε, see Figure 17. Then the curves of the corresponding different ε-values do overlap. This action corresponds to a proceeding in which we neglect the constant term in the Taylor expansion of ζ_3^2 with respect to x_2 around $x_2 = 0$, hence starting with the linear term as in the hard clamped situation. Then of course we would have $m = 2$ analogously to the hard clamped case, which reveals that we have indeed only one power of ε deviation in the asymptotic expansions and the other power is due to the evaluation of the functionals with respect to the 'wrong' variable.

The reason for the dramatic change in the asymptotic expansion depending on the lateral boundary conditions is exclusively due to the presence of the Kirchhoff–Love term ζ_3^2 in the free situation. This fact is verified by the two graphs in Figures 18 and 19, where we show the behaviour of the functional $J_3[u_3, P_2]$ for hard clamped and free lateral boundary

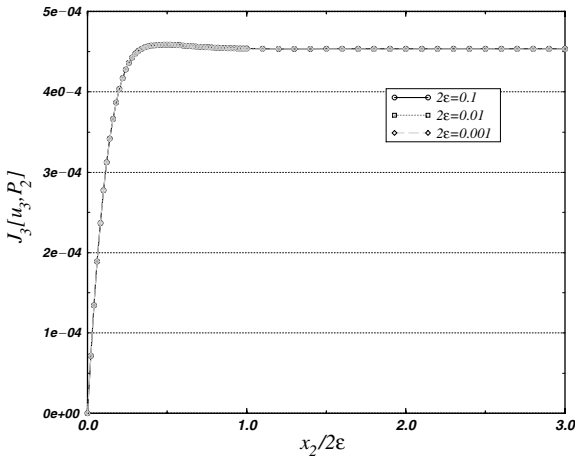

Figure 18. Hard clamped $J_3[u_3, P_2]$.

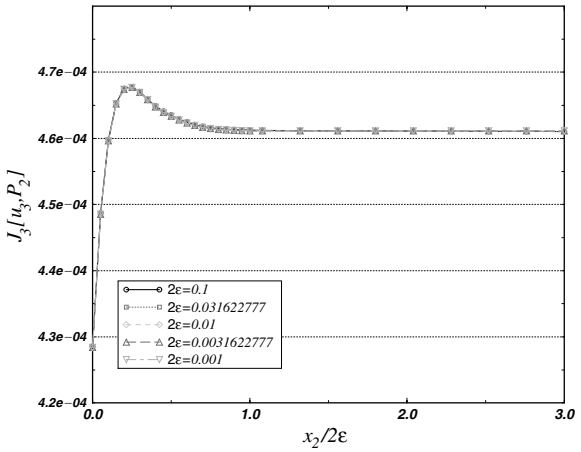

Figure 19. Free $J_3[u_3, P_2]$.

conditions. Let us recall that the Kirchhoff–Love terms are orthogonal to P_2 and thus are invisible in $J_3[u_3, P_2]$. We see that apart from the boundary layer profiles which clearly have to differ from each other, the same behaviour independent of the lateral boundary conditions is noticed. In both cases $J_3[u_3, P_2]$ tends to the same constant as we move away from the boundary layer zone which is due to the presence of $\mathfrak{H}_3$.

5. CONCLUSIONS

We have shown that there exist loading conditions applied to three-dimensional plate thin elastic structures, for which the leading term in the asymptotic solution (as thickness tends to

zero) vanish (the limit Kirchhoff–Love displacement is zero). However, this does not mean that the three-dimensional displacements are zero and the knowledge of a number of terms in the asymptotic expansion is necessary if one wants to understand the nature of the response of the thin structure. Contrary to the standard case, the first non-zero term combines in general a Kirchhoff–Love displacement with a boundary layer term and a displacement resulting from higher-order moments of the loading.

We can quantify this fact by an evaluation of the orders of magnitude of the elastic energy $\int_\Omega [A]\mathbf{e}(\mathbf{u}) : \mathbf{e}(\mathbf{u})$ of the different terms involved in standard and higher-order responses. For a standard response, the energy of the limit Kirchhoff–Love displacement is $\mathcal{O}(\varepsilon)$, like that of the further term $\varepsilon\mathbf{v}^1$ (see (7), (10) and (11)), and the boundary layer term $\varepsilon\boldsymbol{\varphi}^1$ has a $\mathcal{O}(\varepsilon^2)$ energy. But for a response of order 2, the energy of the Kirchhoff–Love displacement is $\mathcal{O}(\varepsilon^5)$, less than the energy of $\varepsilon^2\mathbf{v}^2$ which is $\mathcal{O}(\varepsilon^3)$, and still less than the energy of $\varepsilon^2\boldsymbol{\varphi}^2$ which is $\mathcal{O}(\varepsilon^4)$ (see (3.1)). The comparison is similar for responses of order 3.

Concerning the loading cases that we numerically investigated, computations were always in accordance with the structure of the first non-zero term in the asymptotics as forecast by the theory. From the practical point of view, it is important to realize that bending loading conditions may exist such that the vertical displacement does not approach infinity as the thickness of the plate tends to zero (Kirchhoff–Love behaviour), but may even approach to zero.

Thus, higher-order responses yield less energetic displacements (the energy has the same behaviour than in the case when the plate is fixed on one of its faces $\Gamma^\pm$). But the maximum energy is concentrated in a boundary layer term and in displacement resulting from higher-order moments of the loading.

From the practical engineering point of view, typical loadings where higher-order responses are excited may be very rare. A clamped thin plate on an airplane or a thin spoiler on a car may be subjected due to the wind to pressure tractions on top and bottom of magnitude ε^2, and if at the same time body forces due to gravitation are of magnitude of ε, then a bending response of order 3, as described in Section 4.1, will be excited.

An important question resulting from the presented analysis is associated with dimensionally reduced plate models, i.e. if one of the explicit bending loading conditions would have been applied to a plate model, would it manifest the higher-order response as the corresponding 3-D plate? Unfortunately, this question remains open (except for the Kirchhoff–Love model which one knows it cannot mimic the boundary layers zone), because the tractions $\mathbf{t}^\pm$ cannot be specified on dimensionally reduced plate models.

APPENDIX

Let us introduce the primitives

$$\oint^{X_3} F \,\mathrm{d}Y_3 := \int_{-1}^{X_3} F(Y_3)\,\mathrm{d}Y_3 - \frac{1}{2}\int_{-1}^{+1}\int_{-1}^{Z_3} F(Y_3)\,\mathrm{d}Y_3\,\mathrm{d}Z_3$$

$$\fint^{Y_3} F \,\mathrm{d}Z_3 := \frac{1}{2}\left(\int_{-1}^{Y_3} F(Z_3)\,\mathrm{d}Z_3 - \int_{Y_3}^{+1} F(Z_3)\,\mathrm{d}Z_3\right)$$

Now we need two functions of the data $(\mathbf{F}, \mathbf{T}^{\pm})$: $\mathfrak{G}$ and $\mathfrak{H}$. These functions are part of formulas giving not only the right-hand sides for ζ^2, see (A4), but also the first non-zero term in the presence of a higher-order response, see Section 3. In the examples that we illustrate, the relevant components of $\mathfrak{G}(\mathbf{F}, \mathbf{T}^{\pm})$ and $\mathfrak{H}(\mathbf{F}, \mathbf{T}^{\pm})$ are simple polynomial functions, see the corollaries in Section 3. The function $\mathfrak{G} = \mathfrak{G}(\mathbf{F}, \mathbf{T}^{\pm})$ is defined in $\mathscr{C}^{\infty}(\bar{\omega} \times [-1,1])^3$ by

$$\mathfrak{G}_3 = 0 \quad \text{and} \quad \mathfrak{G}_*(x_*, X_3) = -\frac{1}{\mu}\left(\oint^{X_3} \left(\fint^{Y_3} \mathbf{F}_* \right) \mathrm{d}Y_3 - X_3 \frac{\mathbf{T}_*^+ - \mathbf{T}_*^-}{2} \right) \tag{A1}$$

The function $\mathfrak{H} = \mathfrak{H}(\mathbf{F}, \mathbf{T}^{\pm})$ is defined in $\mathscr{C}^{\infty}(\bar{\omega} \times [-1,1])^3$ by

$$\mathfrak{H}_3 = -\frac{1}{\lambda + 2\mu}\left(\oint^{X_3} \left(\fint^{Y_3} F_3 \right) \mathrm{d}Y_3 - X_3 \frac{T_3^+ - T_3^-}{2} \right)$$

and

$$\mathfrak{H}_\alpha = -\oint^{X_3} \left(\partial_\alpha \mathfrak{H}_3 + \frac{1}{\mu} Y_3 \mathfrak{F}_\alpha(\mathfrak{G}) + \frac{\lambda}{\mu} \fint^{Y_3} \left\{ \partial_{\alpha 3} \mathfrak{H}_3 - \frac{1}{2} \int_{-1}^{+1} \partial_{\alpha 3} \mathfrak{H}_3 \, \mathrm{d}Z_3 \right\} \right) \mathrm{d}Y_3 \tag{A2}$$

where the operator $\mathfrak{F} : \mathbf{v} \mapsto \mathfrak{F}(\mathbf{v})$ is defined from $\mathscr{C}^{\infty}(\bar{\omega} \times [-1,1])^3$ into $\mathscr{C}^{\infty}(\bar{\omega})^3$ by

$$\mathfrak{F}_\alpha(\mathbf{v}) = \frac{\tilde{\lambda}}{2} \int_{-1}^{+1} \fint^{Y_3} \partial_{\alpha\beta} e_{\beta 3}(\mathbf{v}) \, \mathrm{d}Z_3 \, \mathrm{d}Y_3 \quad \text{and} \quad \mathfrak{F}_3(\mathbf{v}) = \mu \int_{-1}^{+1} \partial_\beta e_{\beta 3}(\mathbf{v}) \, \mathrm{d}Y_3 \tag{A3}$$

$\alpha, \beta = 1, 2$ with double index implying summation.

Finally, the right-hand sides of Equations (14) and (15) for $k = 2$ are given by

$$\mathbf{R}_{\mathrm{m}}^2 = \mathfrak{F}_*(\mathfrak{G}) - \frac{\tilde{\lambda}}{4\mu} \nabla_* ([F_3]_1 + T_3^+ - T_3^-)$$

and

$$R_{\mathrm{b}}^2 = 3\mathfrak{F}_3(\mathfrak{H}) + \frac{3\mu(3\lambda + 4\mu)}{2(\lambda + 2\mu)} \Delta_* \, \mathrm{div}_* [\mathfrak{G}_*]_1 \tag{A4}$$

For further details the reader is referred to Reference [9].

ACKNOWLEDGEMENTS

The third author expresses his gratitude to Profs. W. Wendland and E. Ramm for their invitation to Stuttgart University under Graduiertenkolleg Modellierung und Diskretisierungsmethoden für Kontinua und Strömungen' where this paper was initiated.

REFERENCES

1. Maz'ya VG, Nazarov SA, Plamenevskii BA. *Asymptotische Theorie elliptischer Randwertaufgaben in singulär gestörten Gebieten I*. Mathematische Monographien, Band 82. Akademie Verlag: Berlin, 1991.
2. Maz'ya VG, Nazarov SA, Plamenevskii BA. *Asymptotische Theorie elliptischer Randwertaufgaben in singulär gestörten Gebieten II*. Mathematische Monographien, Band 83. Akademie Verlag: Berlin, 1991.
3. Oleinik OA, Shamaev AS, Yosifian GA. *Mathematical Problems in Elasticity and Homogenization. Studies in Mathematics and its Applications*. North-Holland: Amsterdam, 1992.

4. Nazarov SA, Zorin IS. Edge effect in the bending of a thin three-dimensional plate. *Prikladnaya Matematika Mekhanika* 1989; **53**(4):642–650 (English translation *Journal of Applied Mathematics and Mechanics* 1989; 500–507).
5. Dauge M, Gruais I. Asymptotics of arbitrary order for a thin elastic clamped plate. I: Optimal error estimates. *Asymptotic Analysis* 1996; **13**:167–197.
6. Dauge M, Gruais I. Asymptotics of arbitrary order for a thin elastic clamped plate. II: Analysis of the boundary layer terms. *Asymptotic Analysis* 1998; **16**:99–124.
7. Dauge M, Gruais I, Rössle A. The influence of lateral boundary conditions on the asymptotics in thin elastic plates. *SIAM Journal on Mathematical Analysis* 2000; **31**:305–345.
8. Dauge M, Yosibash Z. Boundary layer realization in thin elastic 3-D domains and 2-D hierarchic plate models. *International Journal of Solids and Structures* 2000; **37**:2443–2471.
9. Dauge M, Djurdjevic I, Rössle A. Higher order bending and membrane responses of thin linearly elastic plates. *Comptes Rendus Hebdomadaises des Seances de l'Academie des Sciences, Série I* 1998; **326**:519–524.
10. Dauge M, Djurdjevic I, Rössle A. Full asymptotic expansions for thin elastic free plates. *Comptes Rendus Hebdomadaises des Seances de l'Academie des Sciences, Série I* 1998; **326**:1243–1248.
11. Ciarlet PG. *Mathematical Elasticity*. vol. II, *Theory of Plates*. North-Holland: Amsterdam, 1997.
12. Rössle A. Asymptotische Entwicklungen für dünne Platten im Rahmen der linearen Elastostatik. *Doctoral Dissertation*, Mathematisches Institut A, Universität Stuttgart, Germany, 1999. On the web: http://www.mathematik.uni-stuttgart.de/mathA/lst6/roessle/ public/Diss.html.
13. Szabó B, Babuška I. *Finite Element Analysis*. Wiley: New York, 1991.

